https://doi.org/10.5194/egusphere-2024-2468
Preprint. Discussion started: 27 August 2024

Tectonic interplay between the South Tibetan Detachment System and the North Himalayan genesis dome

Xinyu Dong,[1,3] Wenhui Li,[1*] Zhanwu Lu,[1] Xingfu Huang,[2] and Rui Gao[1,3]

[1] SinoProbe Laboratory of Ministry of Natural Resources, Institute of Geology, Chinese Academy of Geological Sciences, Beijing 100037, China.

[2] School of Earth Sciences, Guilin University of Technology, Guilin 541006, China.

[3] School of Earth Sciences and Engineering, Sun Yat-sen University, Guangzhou 510275, China

Correspondence to: Wenhui Li (dereklee1984@126.com)

Abstract

The formation and evolution of the Himalayas are intimately linked to the South Tibetan Detachment System (STDS) in the northern Himalayas. Despite ongoing controversies about the deep structural style of the STDS, understanding the emplacement mechanism of the leucogranite in the North Himalayan gneiss domes (NHGDs) remains challenging due to insufficient information about deep structures. In this study, we characterized the subsurface structure of the STDS on the eastern side of the Tethys Himalayas and analyze the relationship between STDS tectonic activity and the formation of the NHGD. We conducted a deep seismic reflection survey with a line length of over 135 km and performed geological field investigations in the eastern Tethys Himalayas (92°E) from 2017 to 2018. Our findings indicate that the STDS presents as a roof thrust fault of duplex structures in the eastern Tethys Himalayas and displays characteristics of two-phase denudation (STDS-1 and STDS-2) from the Miocene, corresponding to the two-phase Tethys tectonic uplift. The first phase of denudation (STDS-1) led to the exposure of its structure around the Yarlhashampo dome. Both STDS-1 and STDS-2 denudation activities play crucial roles in promoting the partial melting of middle crust metasediments, which subsequently migrated upward to form leucogranite through diapirism in the core of the Yarlhashampo dome.

https://doi.org/10.5194/egusphere-2024-2468
Preprint. Discussion started: 27 August 2024

1 Introduction

The formation and evolution history of the Himalayas is intimately linked to the South Tibetan Detachment System (STDS) in the northern Himalayas. Burg and Chen (1984) were the first to uncover the significant north-dipping, low-angle ductile shear belt in the Himalayas between the Greater Himalayan crystalline and Tethys Himalayas, which was later termed as the STDS by Burchfiel et al. (1992). Various geological and geophysical studies on the STDS have been subsequently carried out (e.g., Brown and Nazarchuk, 1993; England and Molnar, 1993; Kellett et al., 2018). Despite these studies, there are still many differing viewpoints regarding the deep structure and formation mechanism of the STDS, making it one of the most controversial first-order structural units in the Himalayas (Kellett et al., 2018; Long et al., 2019; Priestley et al., 2019). England and Molnar (1993) systematically discussed the formation mechanism of the STDS, suggesting that it developed in collisional and compressional environments. Following this, various models have been proposed to understand the kinematics and dynamics of the STDS, including gravity collapse (Burchfiel et al., 1985), channel flow (Hauck et al., 1998; Kellett et al., 2018), lithosphere-scale wedge extrusion (Chemenda et al., 2000) and duplexing (Yin, 2006; He et al., 2016). Overall, the deep structures of STDS are key to constructing geological models related to the system.

Additionally, the STDS is closely linked to the formation of the North Himalayan gneiss domes (NHGDs) (Lee et al., 2000; Beaumont et al., 2004; Yin, 2006). Previous research has revealed that granites occupy the cores of most NHGDs (Jessup et al., 2019). These granites are primarily intrusive acid rocks (leucogranites) with high alumina and high silica-alkali contents, along with some mica granites (Zeng et al., 2011; Wu et al., 2015). Gao et al. (2016a) suggest that fluid-absent melting and fluid-fluxed melting are the primary mechanisms controlling the formation of these granites and the subsequent petrogenesis from the Eocene to late Miocene. However, it remains controversial whether these granites formed through in situ remelting of metapelites (Harrison et al., 1999; Searle et al., 2010) or through ex situ magma anatexis migration and crystallization (Wu et al., 2015; Yang et al., 2019). Further study of the formation and evolutionary relationship between the STDS and NHGDs is crucial for understanding the formation and growth of the Himalayas. Currently, most

https://doi.org/10.5194/egusphere-2024-2468
Preprint. Discussion started: 27 August 2024

information about the Himalayan crustal structure comes from passive source seismic observations with relatively low resolution. However, controlled source imaging can provide a more precise crustal structure (Priestley et al., 2019; Gao et al., 2021; Lu et al., 2022).

In this study, we conducted a deep seismic reflection survey and relevant geological field investigations on the east side of the Himalayas in 2017-2018 (Figs. 1 and 2). The stacked seismic line spans approximately 135 km in length. We described the fine crust structure on the eastern Tethys Himalaya, illustrate the deep structural properties of the STDS, and analyze the formation process of the NHGDs (i.e., Yarlhashampo dome) and its relationship to STDS. Finally, we propose a two-phase uplifting model of the eastern Tethys Himalaya.

2 Geological Background

The extinction of the Neo-Tethys Ocean and the collision between the Indian-Eurasian continents along the Yarlung-Zangbo suture (YZS) gave rise to a primary collision zone. This zone is composed of the southern margin of the Asian Plate, the YZS, the Himalayan orogen, and the northern margin of the Indian Plate. The Gangdese-YZS-Tethys Himalaya region occupies the core area of this complex collision zone.

The Himalayan orogen is composed of Tethys Himalayan sediments (THSs), the Greater Himalayan metamorphic series (GHS), the Lower Himalayan metamorphic series (LHS), and Sub-Himalayan sediments (SHSs), arranged from north to south. The north side of the Tethys Himalayas is constrained by the YZS, while the south side connects with the GHS, bound by the South Tibetan Detachment System (STDS). The Main Central Thrust fault (MCT) separates the Greater and Lower Himalayas, and the Main Boundary Thrust fault (MBT) divides the Lower Himalayas and the Sub-Himalayas. The Main Front Thrust fault (MFT) developed along the southern Sub-Himalayas forms the boundary between the Sub-Himalayas and the Siwalik molasse (Fig. 1; Yin, 2006; Searle et al., 2019). The active age of these regional faults gradually decreases from north to south (Priestley et al., 2019).

https://doi.org/10.5194/egusphere-2024-2468
Preprint. Discussion started: 27 August 2024

The YZS separates the Gangdese magmatic belt from the Tethys Himalayas. This suture zone extends approximately 2500 km from the northern margin of Pakistan and northwestern India to eastern southern Tibet (Searle and Lamont, 2019; Zhang et al., 2014). It is generally believed that this suture zone is the remnant of Neo-Tethys oceanic subduction (Metcalf and Kapp, 2019).

The Gangdese magmatic belt, located north of the YZS, is primarily composed of Late Triassic to Eocene calc-alkaline I-type granitoid batholiths, partially covered by Paleocene to mid-Eocene Linzizong andesitic volcanic rocks. These magmatic rocks formed from the Mesozoic to late Cenozoic (Searle, 2018; Guo et al., 2018; Metcalf and Kapp, 2019; Guo et al., 2021; Lu et al., 2022). Mesozoic magmatism in this belt primarily resulted from the subduction of the Neo-Tethys Ocean (Ma et al., 2018), while Cenozoic magmatism is chiefly associated with the collision of the Indian-Asian plates (Hou et al., 2004). A north-dipping Gangdese thrust fault (GT) developed along the southern margin of the Gangdese magmatic belt and was active during the late Oligocene. The GT thrust a portion of the Gangdese batholith southward onto the Tethys Himalaya (Yin et al., 1994).

The Tethys Himalaya, located south of the YZS, are a subunit on the northernmost side of the Himalayas (Wang et al., 2018) and are composed of Precambrian to Eocene volcanic rocks, marine sediments, and clastics with numerous folds and thrust belts (Long et al., 2019). The average thickness of the crust in the Tethys Himalaya is 70 to 80 km (Aikman et al., 2008; Priestley et al., 2019), and the thickness of the sediments in this area increased from the approximately 10 km to about 20 km due to regional folding during the collision (Cottle et al., 2015). The Tethys Himalaya host important mineral resource exploration areas, where Sn-W rare metal and Sb-Au-Pb–Zn metal deposits have been discovered (Cao et al., 2019; Cao et al., 2020), including a lithium mineral deposit (spodumene pegmatite) reported from Lhozhag (Wang et al., 2023). Affected by the continuous convergence between the Indian and Asian continents, many faults and fold belts have developed in the Tethys Himalaya (Fig. 2; Ratschbacher et al., 1994), such as the STDS, the Lhozhag fault, the Rongbu-Gudui fault, the Lhunze fault, the Qiongduojiang fault, and the Greater Counter Thrust (GCT). These faults are distributed along the orogenic belt in the E-W direction. Among them, the STDS is

https://doi.org/10.5194/egusphere-2024-2468
Preprint. Discussion started: 27 August 2024

a giant detachment system (ca. 2000 km in length). The western part of the STDS detachment is also known as the Zanskar shear zone (Searle and Lamont, 2019). Geological field studies indicate that the STDS exhibits both top-to-north extensional activity and top-to-south thrust activity records, which may be associated with the tectonic activity of the GCT and corresponding metamorphism and/or anatectic events within the Greater Himalaya (Hodges et al., 1996; Webb, 2013; Zhang et al., 2020; Xu et al., 2021). Additionally, Miocene leucogranites exposed along the footwall of the STDS in the Greater Himalaya (Kellett et al., 2018; Zhang et al., 2020) are useful for constraining the active period of the STDS based on prekinematic, synkinematic, and postkinematic relationships (Zhang et al., 2020). Dating results based on the contemporaneous development of leucogranites and the subsequent cut-off records of the STDS suggest that the STDS was mainly active in the early Miocene (Cottle et al., 2015). Some studies suggest that the active depth of the STDS may reach 22-25 km along the orogen, based on metamorphic mineral and geochemical element indicators (Dézes et al., 1999; Chen et al., 2018; Waters et al., 2018; Long et al., 2019; Dong et al., 2021). The south-dipping Great Counter Thrust fault (GCT) developed along the north side of the Tethys Himalaya and was active during the Miocene (Yin, 2006). This fault thrust some Indian continental margin sediments and ophiolitic mélange northward onto the Gangdese magmatic belt (Edwards et al., 1996; Wang et al., 2018). Its roots connect to the STDS on the south side (Yin et al., 1994).

Additionally, the Lhozhag fault is the eastern extension of the Gyirong-Kangmar fault, also known as the Dingri-Gangba fault or Gyirong-Dingri-Gangba-Cuona fault (Zheng et al., 2014). This fault separates the Permian to Early Cretaceous Lhagoi-Kangri passive continental margin basin from the northern Himalayan carbonate platform (Liu et al., 2019). This fault experienced N–S-trending compression in the Paleogene, N–S-trending extension in the Miocene, N–S-trending compression in the Pliocene, and N–S-trending extension with detachment in the Quaternary (Liu et al., 2019). The Rongbu-Gudui fault also underwent northward extension and detachment in the late stage of thrust activity, with a N-NNE strike. The late extension could be attributed to the extrusion of the Greater Himalaya. Since the early Miocene, many N-S-trending rift systems (NSTRs) have developed in the northern Himalayas and the hinterland of the plateau (Yin, 2000), with some rifts still active today, such as the Cuona-Sangri rift and the Yadong-Gulu rift (Armijo et al., 1986).

https://doi.org/10.5194/egusphere-2024-2468
Preprint. Discussion started: 27 August 2024

The North Himalayan gneiss domes (NHGDs) are distributed throughout the Tethys Himalaya (Diedesch et al., 2016; Jessup et al., 2019). These domes are further classified into N-S-oriented NHGDs, which were active during the early to middle Miocene, and E-W-oriented NHGDs, which become active after the middle Miocene (Jessup et al., 2019). The N-S-oriented NHGDs are assumed to be principally associated with the northward expansion of the Himalayas along the STDS. Both Paleozoic orthogneiss and Cenozoic leucogranites have developed within these domes. Representative N-S-oriented NHGDs include the Kangmar, Yarlhashampo, Mabja, Kampa and Malashan domes. The seismic line used in this study traverses the Yalashampo dome (alternatively known as the Yalaxiangbo/Yardoi dome), located at the easternmost terminus of the NHGDs (Aikman et al., 2008; Wang et al., 2018).

The Greater Himalaya sequence (GHS) is a “sandwich”-like metamorphic core situated between the northern Tethys Himalaya and the southern Lower Himalaya. It is primarily composed of Neoproterozoic-Mesozoic amphibolite facies metamorphic rocks and parametamorphic rocks (Searle, 2018; Searle and Lamont, 2019; Wang et al., 2021). The GHS experienced partial melting and magmatic extrusion during the Miocene (Long et al., 2019; Xu et al., 2021).

3 Results

3.1 Geological Investigation

The geological field investigation commenced at the STDS and progressed northward along the reflection seismic exploration route, concentrating on the Lhozhag and Lhunze faults. Investigations were conducted on both the northern and western sides of the Yarlhashampo dome, with particular emphasis on the sinistral thrust faults encircling the dome. Subsequently, the investigation crossed the YZS and the Gangdese magmatic belt (Figs. 2, 3, 4).

https://doi.org/10.5194/egusphere-2024-2468
Preprint. Discussion started: 27 August 2024

The field geological investigation revealed that the Triassic to Cretaceous clastic rocks, along with limestone and mudstone, were exposed in the hanging wall of the STDS. Some shallow metamorphic rocks were also exposed in the study area (Fig. 3B). The primary exposed stratigraphic succession along the seismic reflection profile includes schist and gneiss. In the eastern Tethys Himalaya, some Late Triassic abyssal-subabyssal sediments (turbidite sandstones and slates interspersed with a few limestones containing basalt and some ophiolitic mélanges) are distributed. Many fault-to-fold structures have developed in the Tethys Himalaya as well. The outer core of Yarlhashampo (YLSP) dome is mainly composed of schist, with some quartz boudin structures indicating extensional shear activities (Fig. 3A). The STDS is exposed on the northern side of the YLSP dome, serving as the boundary between the lower and middle structure layer of this dome. Leucogranites with boudinage structures within the STDS indicate a top-to-north shearing movement of the middle structure layer (Fig. 3D; Wang et al., 2018). Granites exposed near the Cuona dome, along with later intrusive activities, has disrupted the overlying schist and gneiss strata (Fig. 3C).

3.2 Seismic Reflection Data

The deep seismic reflection profile described below, spanning approximately 135 km, crosses the eastern Himalayas, an important area for determining the subsurface structures of the STDS and the Yarlhashampo dome (Fig. 1). Dong et al. (2020) previously described the northern part of this seismic profile. This paper presents the complete set of seismic reflection data running north to south across the eastern Himalayas. The data collection and processing methods followed those described by Dong et al. (2020). Four types of explosive active source were employed during the data acquisition, including: (1) single shot holes filled with 48 kg of dynamite at 30 meters depth, spaced 250 meters apart, (2) paired shot holes containing 192 kg of dynamite at 50 meters depth, spaced 1 kilometre apart, (3) shot holts with 500kg of dynamite at 50 meters depth, spaced 3 km, and (4) clusters of 15 shot holes with 2000 kg of dynamite at 50 meters depth, spaced 23 kilometres apart. Seismic arrays comprising 720, 900, and 2000 receivers were utilized to record the four source configurations (single, pair, and cluster shots) within a 30-second two-way travel time

https://doi.org/10.5194/egusphere-2024-2468
Preprint. Discussion started: 27 August 2024

(TWTT) window. The data processing was conducted using the Focus seismic data processing platform. Figure 4A shows the final post-stack migrated profile.

3.3 Shallow Level Seismic Reflection Profile (0-10s, TWT)

3.3.1 South part of seismic reflection profile (STDS section, CMP 87-2087)

Within depths of 0-4 s two-way travel time (TWTT) or approximately 0-12 km (calculated using the average seismic velocity in the crust of 6 km/s along the Himalayas, as previous studies such as Guo et al., 2021 and Lu et al., 2022), a series of reflection wave groups can be observed in the shallow part of the seismic reflection profile. Meanwhile, a series of near-horizontal reflection wave groups extend from the surface down to 7 s TWTT (corresponding to CMP587, marked as ① in Fig. 5B). Since the surface near CMP587 is the exposed position of the regional Lhozhag fault in the study area (Fig. 4C), we infer that this reflection event indicates the regional activity characteristics of the Lhozhag fault. Combined with previous surface geological survey results and the relative dislocation information of strata-based seismic reflectors in the fault's hanging wall and footwall, we can infer that this fault is characterized by top-to-south thrusting. North to CMP1587, similar to the Lhozhag fault, the reflection wave group is dislocated in the depth range of 1-4 s TWTT (marked as ② in Fig. 5B). The reflection wave group on the north side thrusts upward relative to the reflection wave group on the south side. However, we could not identify any obvious faults on the surface of the area. This phenomenon indicates the presence of a north-dipping blind thrust fault formed in the Tethys Himalayan sedimentary strata.

3.3.2 Central part of seismic reflection profile (YLSP section, CMP 2087-5087)

The 0-5 s TWTT depth of CMP2587-4087 exhibits a prominent arcuate reflection wave group feature, corresponding to the Yarlhashampo dome on the surface (Fig. 4B; Zhang et al., 2012). This reflection represents the subsurface structural feature of the Yarlhashampo dome, consistent with the surface geological research results. The dome structure comprises three layers: upper, middle, and lower (Wang et al., 2018).

https://doi.org/10.5194/egusphere-2024-2468
Preprint. Discussion started: 27 August 2024

Near CMP3087, the 0-4 s TWTT reflection wave group (marked as ④ in Fig. 5B) features a south-dipping characteristic around the dome's southern side. In contrast, the reflectors near CMP2087 (marked as ③ in Fig. 5B) adjacent to the dome's southern side gradually transition into a north-dipping feature, which may correspond to variations in the dome's lower detachment as previously interpreted (Dong et al., 2020). The northern side near CMP2087 exhibits subhorizontal reflection (marked as ③ in Fig. 5B) and upward thrusting, while the main reflection feature on the southern side dips northward, potentially indicating another north-dipping thrust fault where the regional Rongbu-Gudui and Lhunze faults are exposed (Zheng et al., 2014). The north-dipping reflection represents the structural style of the Rongbu-Gudui and Lhunze faults.

Notably, the lower detachment layer on the south side of the dome may extend southward to the Lhozhag fault based on changes in the reflection properties of the fault hanging wall and footwall. This fault is thrust and dislocated by blind faults in the Tethys Himalaya. Geological and geophysical evidence suggests that the dome's lower detachment represents the exposure of the STDS in the Tethys Himalayan domain (Fig. 4B; Yan et al., 2012; Zhang et al., 2012; Wang et al., 2018). Thus, part of the STDS is revealed in the CMP2587-4087 (~3 s TWTT) range of this seismic profile (marked as ⑤ in Fig. 5B).

The interpretation of the lower detachment structure on the northern side of the dome (Wang et al., 2018) suggests that the reflection wave group corresponding to this detachment structure is truncated by the Jiama-Zongxu-Qusang regional blind thrust fault (near CMP3587, ~3 s TWTT, marked as ⑥ in Fig. 5B). The reflection characteristics of this thrust fault can be traced northward to CMP4087 (depth ~3 s TWTT). As we tracing the reflection characteristics of the lower detachment layer under the dome to the north, the reflection wave group gradually becomes gentle and slightly inclined to the south, extending to the vicinity of CMP 4587.

https://doi.org/10.5194/egusphere-2024-2468
Preprint. Discussion started: 27 August 2024

In the depth range of 4-6 s TWTT, a prominent "bright spot" reflection can be observed in the reflection profile corresponding to CMP2087-2587 and CMP4587-5087. This reflection feature is comparable to the "bright spot" features observed in the IN-DEPTH seismic reflection profile (Hauck et al., 1998), exhibiting similar depth and amplitude characteristics. Additionally, these features are characterized by low resistivity and high conductivity in magnetotelluric data (e.g., Spratt et al., 2005, IN-DEPTH line-700 in Fig. 1), corresponding to the transition range between negative and positive impedance in nearby receiver function data (Shi et al., 2015). These "bright spot" reflections may indicate regional partial melts (Nelson et al., 1996).

Previous studies have revealed that partial melting of deep metasediment was the primary formation mechanism of these melts during the thickening process of the Tethys Himalaya (Searle et al., 2018). Metamorphism and dehydration in the Lower Himalaya, along with free water from Tethys Himalayan sediments, resulted in fluids that entered the Greater Himalaya, metasomatizing nearby metamorphic rocks. This process was accompanied by depressurization and upwelling of asthenospheric materials, and a rise in crustal temperature due to the accumulation of radioactive heat. Consequently, partial melting of meta-argillaceous rocks occurred in the Greater Himalaya during the Miocene, particularly at the junction of the overlying plate and the thrust plate (Guo et al., 2012; Gao et al., 2016a). Furthermore, early STDS extension activity (Zhang et al., 2012) and late N-S-trending rift activity (Zeng et al., 2017) promoted decompression melting in this area. Therefore, the partial melts represented by the "bright spot" reflections in this study are likely related to the N-S rifting activity that has persisted to the present day.

A distinct wave group can be traced continuously from the southernmost area to the middle of the seismic reflection profile (CMP87 to CMP4087, 4-9 s TWTT, marked as ⑦, ⑧, ⑨, ⑩ in Fig. 5B). This wave group is interrupted and staggered by the Lhozhag fault (marked as ① in Fig. 5B) near CMP1337, and those wave groups under this seismic reflection exhibit north-dipping characteristics. By integrating the regional tectonic features (Yin, 2006; Kellett and Grujic, 2012), deep seismic reflection profiles from the western and central Himalayas (Hauck et al., 1998; Gao et al., 2016b), receiver function results from the eastern Himalayas

https://doi.org/10.5194/egusphere-2024-2468
Preprint. Discussion started: 27 August 2024

(Shi et al., 2015), and previous studies on the dynamic depth range of the STDS in the central Himalayas (Waters et al., 2018), we interpreted this reflection wave group as a feature of the current STDS recorded in the seismic reflection profile. To comprehensively understand this, the STDS structure presented in the seismic reflection profile was extended southward to the location of the surface exposure of the STDS in the study area (Fig. 1).

Unlike the previously interpreted STDS structure (hereafter referred to STDS-1 for clarity, corresponding to the South Tibet thrust system, e.g., Zhang et al., 2020; Xu et al., 2021), which appears within the range of CMP887-4087 (~3 s TWTT, marked as ⑤ in Fig. 5B), this reflection feature (CMP87 to CMP4087, 4-9 s TWTT, marked as ⑦, ⑧, ⑨, ⑩ in Fig. 5B) is more continuous. Its amplitude is more prominent, indicating it represents a second stage record of the STDS activity (STDS-2).

3.3.3 North part of seismic reflection profile (YZS section, CMP 5087-6637)

Further toward the northern part of the profile, arc-shaped transparent reflections beneath the Gangdese magmatic area are predominantly observed. The regional GCT was exposed near CMP5087 on the surface. In this reflection profile, the top of its footwall dips southward, extending to CMP4087 (~3 s TWTT, marked as ⑪ in Fig. 5B) in the south. A series of south-dipping reflections can also be observed from the north side of the exposed GCT location to CMP5587, corresponding to the reflection characteristics of the Yarlung-Zangbo ophiolite suite exposed on the surface (Figs. 4, 5D). The thrusting and dislocation phenomena of the reflection wave group north of CMP5587 are interpreted as features of the GT fault (marked as ⑫ in Fig. 5B). Simultaneously, the intermittent reflection characteristics of the Gangdese magmatic arc and the lower crust of the Lhasa terrane at ~9 s TWTT in the northern YZS may represent a ductile shear zone (marked as ⑬ in Fig. 5B). The 0-4 s TWTT depth range of the Tethys Himalayan sedimentary system exhibits significant reflection wave group reformation or deformation, primarily related to tectonic faulting and folding due to the India-Asia plate convergence and orogen thickening (Searle, 2018).

https://doi.org/10.5194/egusphere-2024-2468
Preprint. Discussion started: 27 August 2024

3.4 Deep Level Seismic Reflection Profile (10-30s, TWT)

For the multiple sets of north-dipping reflection wave groups presented below the STDS-1, Guo et al. (2021) interpreted these reflections as duplexing structures of the southward thrusting upper Indian crust materials, which decoupled from the lower Indian crust in the early Eocene during Himalayas uplifting (Searle, 2018). In the northern part of this profile, Dong et al. (2020) observed specific angle changes in the reflection characteristics and interpreted these as the reflection characteristics of different fault-bound horst blocks during duplexing. Similarly, the multiple sets of north-dipping reflection features below the STDS in this profile further represent duplex structures formed during the convergence of the Indian and Asian plates, recording a superimposition of fault-bound horst blocks at various crustal scales (Fig. 6). Meanwhile, STDS-2 is interpreted as the roof thrust fault of the current duplexing structure (He et al., 2016).

For the duplexing structures in our seismic reflection profile, the series of fault-bound horst blocks (Fig. 6) are further divided based on the cutting relationship between reflection wave groups or change in reflection characteristics. The central fault-bound horst block (6-14s TWTT, CMP2587-CMP3587) is primarily a near-transparent reflection area. Based on the interpretation of transparent reflection areas in other deep seismic reflection profiles (e.g., Zhang et al., 2014; Guo et al., 2021) and exposed Mid-Eocene high Sr/Y granites on the surface, which originate from partially melted mafic rocks of the lower crust (Zeng et al., 2011; Zeng et al., 2017), we think this fault-bound horst block represents crystalline magmatic rocks. It was a very large fault-bound horst block during the India-Asia collision and compression due to the significant strength difference between the fault block and the surrounding rocks.

For this type of crustal-scale duplexing structure, interstitial fluid pressure is highly effective in reducing the compressive stress and frictional resistance of the fault surface between plates (Hubbert and Rubey, 1961). There is a boundary between the reflection characteristics of middle crust duplexing structures and the intense reflection in the lower crust from 12 s TWTT in the southern part to 18 s TWTT below CMP4087 in the north. Based on receiver

https://doi.org/10.5194/egusphere-2024-2468
Preprint. Discussion started: 27 August 2024

function seismic data (Shi et al., 2015; Schulte-Pelkum et al., 2019) and deep seismic reflection profiles (Nelson et al., 1996) in the adjacent area, we think that this reflection feature represents the MHT between the subducted Indian plate and the overlying Asian plate.

Additionally, the contact area between the Indian plate and Lhasa terrane (CMP4087-5087, 8-20 s TWTT) is characterized by intermittent and irregular reflection, representing the accretion of wedge material from the overlying sedimentary layer of the subduction plate and oceanic crust fragments during collision and convergence. This area may also serve as the main channel for mantle fluid migration to the upper crust.

The material of the subducted lower crust of India, decoupled from the upper crust, is mainly characterized by short-axis reflection with a faint northward dip. The reflection beneath the shear zone at ~9 s TWTT on the north side of the YZS is not visible, with only a very small south-dipping reflection observed. Combined with petrological and geophysical data, it is considered that the main reflection features in this area were transformed during the upwelling of mantle material and partial melting of the lower crust, indicating a hotter tectonic environment (Xie et al., 2016).

The Moho reflection is visible at the bottom of the lower crust as an intense reflection on the southern side of the YZS, evident in the range of CMP587-1587 corresponding to 22-24 s TWTT on the south side of the seismic reflection profile. It extends northward intermittently to a depth of ~25 s TWTT (approximately 75 km deep, calculated using a crustal average velocity of 6 km/s), corresponding to CMP5337, which is close to twice the average global crustal thickness.

The reflection characteristics of the lower crust base boundary of the Lhasa terrane on the northern side of the YZS can be vaguely observed when tracing the seismic reflectors down

https://doi.org/10.5194/egusphere-2024-2468
Preprint. Discussion started: 27 August 2024

to a depth of approximately 24 s TWTT. Although the Moho reflection interface is not readily apparent, when combined with other geophysical research data from the surrounding area (Singer et al., 2017; Schulte-Pelkum et al., 2019), the seismic reflection facies representing the Moho of the Lhasa terrane can still be identified at a depth of ~24 s TWTT. At the same time, the Moho of the Indian plate and Lhasa terrane converge near ~25 s TWTT of CMP5337, which may represent the position of the "mantle suture zone" (Klemperer et al., 2013).

4 Discussion

4.1 Eastern Himalayas Uplift Mechanism

The uplift mechanism of the Himalayas is categorized into two main models: the "extrusion model" (Burchfiel and Royden, 1985) and the "duplexing model" (Webb, 2013). Both hypotheses have specific requirements for the structural style of the STDS. According to He et al. (2016), in the extrusion model, the STDS plays a role as a normal fault, with its hanging wall slipping along the STDS and exhibiting a typical fault displacement greater than 10 km. In the duplexing model, the STDS primarily acts as a back-thrust fault, with its southern end terminating at the MCT and its northern end potentially connecting to the GCT. Alternatively, the STDS may serve as a roof thrust fault during the evolution process, particularly at certain stages of crustal thickening (Yin, 2006; Webb, 2013).

Previous studies also show that the STDS has complex characteristics due to its multistage extensional-compressional activities. For example, the STDS near the Yarlhashampo dome exhibited features of a compressional structure before the extensional activities (Zhang et al., 2012; Chen et al., 2018). Similarly, the STDS in the Zanskar area experienced SW-trending synmetamorphic thrusting in the early stage and NE-trending extension after early-stage thrust activities in the late phase (Dézes et al., 1999). The STDS exposed in the Gyirong area transitioned from southward compressional thrusting to northward extensional detachment in the late Eocene, while tectonic activity shifted from extensional detachment to compressional thrusting in the early Miocene (Zhang et al., 2012). In the Khula-Kangri area, early STDS

https://doi.org/10.5194/egusphere-2024-2468
Preprint. Discussion started: 27 August 2024

extension activities underwent further N-S extension following relative denudation due to plutonism (Edwards et al., 1996). Observations of the Annapurna fault and Kalopani shear zone (ADF and KSZ, branches of the STDS) in the Thakkola area of central Nepal suggest a thrusting thickening event between early and late extensional detachment in the Miocene and corresponding GHS exhumation events (Brown et al., 1993; Xu et al., 2021).

Combining the regional geological background and the results obtained in this study, we believe that the STDS in our study area underwent a multistage extension and compression transformation process (Fig. 7). Due to footwall decompression melting (accompanied by magma upwelling and diapir formation) caused by the gravity collapse of STDS-1, which formed by duplexing in the Eocene (Fig. 7B-a), and the northward thrusting and faulting of the north-dipping Lhozhag fault, STDS-1 was exposed around the Yarlhashampo dome. STDS-1 was eroded in the later stage of evolution (Fig. 7B-b). With the continuous collision and compression of the Indian and Asian plates, duplexing continued to cause crustal thickening of the Himalayas. The detachment process along the STDS was redeveloped (STDS-2) in areas with high-temperature and high-pressure conditions, similar to the early activity during the middle to late Miocene (Fig. 7B-b). STDS-2 became the new roof thrust fault of duplexes. STDS-2 underwent a denudation process similar to STDS-1 at a later stage (Fig. 7B-c) because the Lhozhag fault has extended in the N-S direction since the Pliocene (Liu et al., 2019), indicating that the study area is now in an extensional environment.

4.2 Gneiss Dome and Leucogranite

The formation mechanism of the N-S gneiss domes in the North Himalayas has long been a research hotspot. Various models have been proposed, including magma diapirism (LeFort et al., 1987), domes or anticlines representing metamorphic core complexes (Chen et al., 1990), out-of-sequence thrusting (Lee et al., 2000), ductile material migrating towards the southern Himalayan margin (channel flow model) (Beaumont et al., 2004), and the duplexing model (Yin, 2006). Overall, these NS-NHGD formation models are related to the GHS southward extrusion (Jessup et al., 2019).

https://doi.org/10.5194/egusphere-2024-2468
Preprint. Discussion started: 27 August 2024

Recent studies further suggest that the NHGDs are metamorphic core complexes formed in a compressional environment, not directly related to crustal extension and magma diapir emplacement (Searle and Lamont, 2019). Our research proposes that the formation of the Yarlhashampo dome is intrinsically linked to the activities of the STDS and the upward thrust of the Lhozhag fault. Based on the structural properties of the Lhozhag fault and the STDS (Fig. 8), during the Paleocene to early Miocene, the retreat and delamination of the Tethys Ocean lithospheric plate during the Indian plate subduction led to the upwelling of lighter, hotter asthenosphere material. This resulted in partial melting dominated by amphibolite/biotite dehydration during the thickening of lower crustal mafic rocks, producing high Sr/Y and high Na/K mica granites that were eventually exposed on the surface (Zeng and Gao, 2017).

Subsequently, STDS-1 gradually developed in the weak tectonically active area of the northern Himalayas, forming a deep ductile shear zone at the front (Lee et al., 2000). Due to the high strain rate of STDS-1 and the influence of the extrusion of middle crustal rocks caused by the ongoing collision process and upwelling of lower crust melt in the Paleocene, STDS-1 continued extending northward into the deep crust. During the Miocene, the extension of STDS-1 ceased (Fig. 8A; Wagner et al., 2010), and concurrently, the Lhozhag fault gradually developed northward along the weak tectonically active area (Liu et al., 2019). In the middle Miocene, the Lhozhag fault was thrust southward due to the Greater Himalayan duplexing, resulting in the denudation of part of STDS-1 located on the Lhozhag fault hanging wall.

Meanwhile, duplex thickening and gravity collapse continued, leading to the gradual development of STDS-2. This caused further partial melting of metasedimentary rocks and the formation of dehydrated muscovite partial melts with low Sr/Yb and high Rb/Sr ratios (Zeng et al., 2011). These melts migrated upward, diapirically reforming the STDS-1 extensional structure and resulting in the formation of the Yarlhashampo dome and the main leucogranite cropping out in its core (Fig. 8B). Notably, the STDS as a whole serves as a

https://doi.org/10.5194/egusphere-2024-2468
Preprint. Discussion started: 27 August 2024

passive roof thrust structure, i.e., the Yarlhashampo dome primarily formed due to STDS activity. The granites exposed in its core mainly result from the decompression melting related to the activities of STDS. The ongoing duplexing transformed the structural style of STDS-2 and led to the dislocation of STDS-1 by further thrusting activities (e.g., the development of the Rongbu-Gudui fault and the Jiama-Zongxu-Qusang fault) (Fig. 8C).

5 Conclusion

Based on a deep seismic reflection profile survey and geological field investigation in the eastern Himalayas (92°E), we discovered that the South Tibet Detachment System (STDS) exhibits characteristics of multistage tectonic activity in the eastern Tethys Himalayas. A primary detachment system developed on the periphery of the Yarlhashampo dome has been revealed, representing an early record of STDS activity (corresponding to the STDS-1 stage). We believe that the activity of the regional Lhozhag fault and STDS contributed to the formation of the Yarlhashampo dome. Consequently, we propose a multi-phase denudation model for the evolution of the STDS in the study area.

Data Availability Statement

Digital elevation map used in this study are open-access and calculated from Global Mapper® platform "https://www.bluemarblegeo.com/knowledgebase/global-mapper-24-1/GlobalMapper.htm". The unprocessed seismic shot gathers and processed stacked SEGY seismic reflection profile are available on request from corresponding author: dereklee1984@126.com.

Conflicts of Interest

The authors declare that there is no conflict of interest regarding the publication of this article.

https://doi.org/10.5194/egusphere-2024-2468
Preprint. Discussion started: 27 August 2024

Funding Statement

This research was supported by the National Natural Science Foundation of China (grant numbers 42174124) and the China Geological Surveying Project (DD20221647, DD20190016).

Acknowledgments

We deeply mourn the passing of Prof. An Yin and express our profound gratitude for his invaluable guidance throughout this study. We are also grateful to our colleagues for their assistance in conducting geological field investigations and collecting seismic data for this study.

References

Aikman, A. B., Harrison, T. M., & Lin, D. (2008). Evidence for early (> 44 Ma) Himalayan crustal thickening, Tethyan Himalaya, southeastern Tibet. Earth and Planetary Science Letters, 274, 14-23.

Armijo, R., Tapponnier, P., Mercier, J. L., & Han, T. L. (1986). Quaternary extension in southern Tibet: Field observations and tectonic implications. Journal of Geophysical Research: Solid Earth, 91, 13803-13872.

Beaumont, C., Jamieson, R. A., Nguyen, M. H., & Medvedev, S. (2004). Crustal channel flows: 1. Numerical models with applications to the tectonics of the Himalayan ‐ Tibetan orogen. Journal of Geophysical Research: Solid Earth, 109, B06406.

Burg, J. P., & Chen, G. M. (1984). Tectonics and structural zonation of southern Tibet, China. Nature, 311, 219-223.

Burchfiel, B. C., & Royden, L. H. (1985). North-south extension within the convergent Himalayan region. Geology, 13, 679-682.

Burchfiel, B. C., Zhiliang, C., Hodges, K. V., Yuping, L., Royden, L. H., & Changrong, D. (1992). The South Tibetan detachment system, Himalayan orogen: Extension contemporaneous with and parallel to shortening in a collisional mountain belt. Geological Society of America, Special Papers, 269.

https://doi.org/10.5194/egusphere-2024-2468
Preprint. Discussion started: 27 August 2024

Brown, R. L., & Nazarchuk, J. H. (1993). Annapurna detachment fault in the Greater Himalaya of central Nepal. Geological Society, London, Special Publications, 74, 461-473.

Cao, H., Li, G., Zhang, Z., Zhang, L., Dong, S., Xia, X., Liang, W., Fu, J., Huang, Y., Xiang, A., and Qing, C. (2020). Miocene Sn polymetallic mineralization in the Tethyan Himalaya, southeastern Tibet: A case study of the Cuonadong deposit. Ore Geology Reviews, 119, 103403.

Cao, H., Zou, H., Bagas, L., Zhang, L., Zhang, Z., & Li, Z. (2019). The Laqiong Sb–Au deposit: Implications for polymetallic mineral systems in the Tethys–Himalayan zone of southern Tibet, China. Gondwana Research, 72, 83-96.

Chemenda, A. I., Burg, J. P., & Mattauer, M. (2000). Evolutionary model of the Himalaya–Tibet system: geopoem: based on new modelling, geological and geophysical data. Earth and Planetary Science Letters, 174, 397-409.

Chen, J., Carosi, R., Cao, H., Montomoli, C., Iaccarino, S., Langone, A., & Li, G. (2018). Structural setting of the Yalaxiangbo dome, SE Tibet (China). Italian Journal of Geosciences, 137, 330-347.

Chen, Z., Liu, Y., Hodges, K. V., Burchfiel, B. C., Royden, L. H., & Deng, C. (1990). The Kangmar Dome: a metamorphic core complex in southern Xizang (Tibet). Science, 250, 1552-1556.

Cottle, J. M., Larson, K. P., & Kellett, D. A. (2015). How does the mid-crust accommodate deformation in large, hot collisional orogens? A review of recent research in the Himalayan orogen. Journal of Structural Geology, 78, 119-133.

Dézes, P. J., Vannay, J. C., Steck, A., Bussy, F., & Cosca, M. (1999). Synorogenic extension: Quantitative constraints on the age and displacement of the Zanskar shear zone (northwest Himalaya). Geological Society of America Bulletin, 111, 364-374.

Diedesch, T. F., Jessup, M. J., Cottle, J. M., & Zeng, L. (2016). Tectonic evolution of the middle crust in southern Tibet from structural and kinematic studies in the Lhagoi Kangri gneiss dome. Lithosphere, 8, 480-504.

Dong, H., Larson, K. P., Kellett, D. A., Xu, Z., Li, G., Cao, H., Yi, Z., & Zeng, L. (2021). Timing of slip across the South Tibetan detachment system and Yadong–Gulu graben, Eastern Himalaya. Journal of the Geological Society, 178, jgs2019-197.

Dong, X., Li, W., Lu, Z., Huang, X., & Gao, R. (2020). Seismic reflection imaging of crustal deformation within the eastern Yarlung-Zangbo suture zone. Tectonophysics, 780, 228395.

Edwards, M. A., Kidd, W. S., Li, J., Yue, Y., & Clark, M. (1996). Multi-stage development of the southern Tibet detachment system near Khula Kangri. New data from Gonto La. Tectonophysics, 260, 1-19.

England, P., & Molnar, P. (1993). Cause and effect among thrust and normal faulting, anatectic melting and exhumation in the Himalaya. Geological Society, London, Special Publications, 74, 401-411.

Gao, L., Zeng, L., & Asimow, P. D. (2016a). Contrasting geochemical signatures of fluid-absent versus fluid-fluxed melting of muscovite in metasedimentary sources: The Himalayan leucogranites. Geology, 45, 39-42.

Gao, R., Lu, Z., Klemperer, S. L., Wang, H., Dong, S., Li, W., & Li, H. (2016b). Crustal-scale duplexing beneath the Yarlung Zangbo suture in the western Himalaya. Nature Geoscience, 9, 555-560.

Gao, R., Zhou, H., Guo, X., Lu, Z., Li W., Wang, H., Li, H., Xiong, X., Huang, X., Xu, X. (2021). Deep seismic reflection evidence on deep processes of tectonic construction of the Tibetan Plateau, Earth Science Frontiers, 28, 320.

Guo, X., Gao, R., Zhao, J., Xu, X., Lu, Z., Klemperer, S. L., & Liu, H. (2018). Deep-seated lithospheric geometry in revealing collapse of the Tibetan Plateau. Earth-Science Reviews, 185, 751-762.

Guo, X., Li, C., Gao, R., Li, S., Xu, X., Lu, Z., Li, W., & Xiang, B. (2021). The India-Eurasia Convergent System: Late Oligocene to Early Miocene passive roof thrusting driven by deep-rooted duplex stacking. Geosystems and Geoenvironment.

Guo, X., Li, W., Gao, R., Xu, X., Li, H., Huang, X., Ye, Z., Lu, Z., & Klemperer, S. L. (2017). Nonuniform subduction of the Indian crust beneath the Himalayas. Scientific Reports, 7, 1-8.

Guo, Z., & Wilson, M. (2012). The Himalayan leucogranites: constraints on the nature of their crustal source region and geodynamic setting. Gondwana Research, 22, 360-376.

Harrison, T. M., Grove, M., Lovera, O. M., Catlos, E. J., & D'Andrea, J. (1999). The origin of Himalayan anatexis and inverted metamorphism: Models and constraints. Journal of Asian Earth Sciences, 17, 755-772.

Hauck, M. L., Nelson, K. D., Brown, L. D., Zhao, W., & Ross, A. R. (1998). Crustal structure of the Himalayan orogen at ~90°east longitude from Project INDEPTH deep reflection profiles. Tectonics, 17, 481-500.

He, D., Webb, A. A. G., Larson, K. P., & Schmitt, A. K. (2016). Extrusion vs. duplexing models of Himalayan mountain building 2: The South Tibet detachment at the Dadeldhura klippe. Tectonophysics, 667, 87-107.

Hodges, K. V., Parrish, R. R., & Searle, M. P. (1996). Tectonic evolution of the central Annapurna range, Nepalese Himalayas. Tectonics, 15, 1264-1291.

Hou, Z., Gao, Y., Qu, X., Rui, Z., & Mo, X. (2004). Origin of adakitic intrusives generated during mid-Miocene east–west extension in southern Tibet. Earth and Planetary Science Letters, 220, 139-155.

Hubbert, M.K., & Rubey, W. W. (1961). Role of fluid pressure in mechanics of overthrust faulting: I. Mechanics of fluid-filled porous solids and its application to overthrust faulting. Geological Society of America Bulletin, 70, 115-166.

https://doi.org/10.5194/egusphere-2024-2468
Preprint. Discussion started: 27 August 2024

Jessup, M. J., Langille, J. M., Diedesch, T. F., & Cottle, J. (2019). Gneiss Dome Formation in the Himalaya. Geological Society London, 15.

Kapp, P., & DeCelles, P. G. (2019). Mesozoic–Cenozoic geological evolution of the Himalayan-Tibetan orogen and working tectonic hypotheses. American Journal of Science, 319, 159-254.

Kellett, D. A., Cottle, J. M., & Larson, K. P. (2018). The South Tibetan Detachment System: history, advances, definition and future directions. Geological Society, London, Special Publications, 483, 377-400.

Kellett, D. A., & Grujic, D. (2012). New insight into the South Tibetan detachment system: Not a single progressive deformation. Tectonics, 31.

Klemperer, S. L., Kennedy, B. M., Sastry, S. R., Makovsky, Y., Harinarayana, T., & Leech, M. L. (2013). Mantle fluids in the Karakoram fault: Helium isotope evidence. Earth and Planetary Science Letters, 366, 59-70.

Lee, J., Hacker, B. R., Dinklage, W. S., Wang, Y., Gans, P., Calvert, A., & McClelland, W. (2000). Evolution of the Kangmar Dome, southern Tibet: Structural, petrologic, and thermochronologic constraints. Tectonics, 19, 872-895.

LeFort, P., Cuney, M., Deniel, C., France-Lanord, C., Sheppard, S. M. F., Upreti, B. N., & Vidal, P. (1987). Crustal generation of the Himalayan leucogranites. Tectonophysics, 134, 39-57.

Liu S., Xia T., Wu M., Wu, M., Zhou, J., Wang, Y., & Wei, M. (2019). Structural Features and Geological Significance of Lhozhag Fault in Lhozhag Area, Southeastern Tibet. Geoscience, 33, 1-12.

Long, S. P., Mullady, C. L., Starnes, J. K., Gordon, S. M., Larson, K. P., Pianowski, L. S., Miller, R. B., & Soignard, E. (2019). A structural model for the South Tibetan detachment system in northwestern Bhutan from integration of temperature, fabric, strain, and kinematic data. Lithosphere, 11, 465-487.

Lu, Z., Guo, X., Gao, R., Murphy, M.A., Huang, X., Xu, X., Li, S., Li, W., Zhao, J., Li, C. & Xiang, B. (2022) Active construction of southernmost Tibet revealed by deep seismic imaging. Nature communications. 13, 3143–3143.

Ma, X., Meert, J., Xu, Z., & Zhao, Z. (2018). The Jurassic Yeba Formation in the Gangdese arc of S. Tibet: Implications for upper plate extension in the Lhasa terrane. International Geology Review, 61, 481-503.

Metcalf, K., & Kapp, P. (2019). History of subduction erosion and accretion recorded in the Yarlung Suture Zone, southern Tibet. Geological Society, London, Special Publications, 483, 517-554.

Nelson, K. D., Zhao, W., Brown, L. D., Kuo, J., Che, J., Liu, X., Klemperer, S. L., Makovsky, Y., Meissner, R. M., Mechie, J., Kind, R., Wenzel, F., Ni, J., Nabelek, J., Chen, L., Tan, H., Wei, W., Jones, A. G., Booker, J., Unsworth, M., Kidd, W. S. F., Hauck, M.,

https://doi.org/10.5194/egusphere-2024-2468
Preprint. Discussion started: 27 August 2024

Alsdorf, D., Ross, A., Cogan, M., Wu, C., Sandvol, E., & Edwards, M. (1996). Partially molten middle crust beneath southern Tibet: Synthesis of project INDEPTH results. Science, 274, 1684-1688.

Priestley, K., Ho, T., & Mitra, S. (2019). The crustal structure of the Himalaya: A synthesis. Geological Society, London, Special Publications, 483, 483-516.

Ratschbacher, L., Frisch, W., Liu, G., & Chen, C. (1994). Distributed deformation in southern and western Tibet during and after the India-Asia collision. Journal of Geophysical Research: Solid Earth, 99, 19917-19945.

Schulte-Pelkum, V., Monsalve, G., Sheehan, A. F., Shearer, P., Wu, F., & Rajaure, S. (2019). Mantle earthquakes in the Himalayan collision zone. Geology, 47, 815-819.

Searle, M. P. (2018). Timing of subduction initiation, arc formation, ophiolite obduction and India–Asia collision in the Himalaya. Geological Society, London, Special Publications, 483, 19-37.

Searle, M. P., Cottle, J. M., Streule, M. J., & Waters, D. J. (2010). Crustal melt granites and migmatites along the Himalaya: melt source, segregation, transport and granite emplacement mechanisms. Earth and Environmental Science Transactions of the Royal Society of Edinburgh, 100, 219-233.

Searle, M. P., & Lamont, T. N. (2019). Compressional metamorphic core complexes, low-angle normal faults and extensional fabrics in compressional tectonic settings. Geological Magazine, 157, 101-118.

Shi, D., Wu, Z., Klemperer, S. L., Zhao, W., Xue, G., & Su, H. (2015). Receiver function imaging of crustal suture, steep subduction, and mantle wedge in the eastern India–Tibet continental collision zone. Earth and Planetary Science Letters, 414, 6-15.

Singer, J., Kissling, E., Diehl, T., & Hetényi, G. (2017). The underthrusting Indian crust and its role in collision dynamics of the Eastern Himalaya in Bhutan: Insights from receiver function imaging. Journal of Geophysical Research: Solid Earth, 122, 1152-1178.

Spratt, J. E., Jones, A. G., Nelson, K. D., Unsworth, M. J., & INDEPTH MT Team. (2005). Crustal structure of the India–Asia collision zone, southern Tibet, from INDEPTH MT investigations. Physics of the Earth and Planetary Interiors, 150, 227-237.

Wagner, T., Lee, J., Hacker, B. R., & Seward, G. (2010). Kinematics and vorticity in Kangmar Dome, southern Tibet: Testing midcrustal channel flow models for the Himalaya. Tectonics, 29.

Wang, J., Hou, K., Yang, L., Liu, X., Wang, R., Li, G., Fu, J., Hu, F., Tian, Y., & Wu, F. (2023). Mineralogy, petrology and PT conditions of the spodumene pegmatites and surrounding meta-sediments in Lhozhag, eastern Himalaya. Lithos, 456, 107295.

Wang, J., Lanari, P., Wu, F., Zhang, J., Khanal, G. P., & Yang, L. (2021). First evidence of eclogites overprinted by ultrahigh temperature metamorphism in Everest East, Himalaya:

https://doi.org/10.5194/egusphere-2024-2468
Preprint. Discussion started: 27 August 2024

Implications for collisional tectonics on early Earth. Earth and Planetary Science Letters, 558, 116760.

Wang, J., Wu, F., Rubatto, D., Liu, K., Zhang, J., & Liu, X. (2018). Early Miocene rapid exhumation in southern Tibet: Insights from P–T–t–D–magmatism path of Yardoi dome. Lithos, 304, 38-56.

Waters, D. J., Law, R. D., Searle, M. P., & Jessup, M. J. (2018). Structural and thermal evolution of the South Tibetan Detachment shear zone in the Mt Everest region, from the 1933 sample collection of LR Wager. Geological Society, London, Special Publications, 478, 335-372.

Webb, A. A. G. (2013). Preliminary balanced palinspastic reconstruction of Cenozoic deformation across the Himachal Himalaya (northwestern India). Geosphere, 9, 572-587.

Wu, F., Liu, Z., Liu, X., & Ji, W. (2015). Himalayan leucogranite: Petrogenesis and implications to orogenesis and plateau uplift: Acta Petrologica Sinica (Yanshi Xuebao), 31, 1-36.

Xie, C., Jin, S., Wei, W., Ye, G., Jing, J., Zhang, L., Dong, H., Yin, Y., Wang, G., & Xia, R. (2016). Crustal electrical structures and deep processes of the eastern Lhasa terrane in the south Tibetan plateau as revealed by magnetotelluric data. Tectonophysics, 675, 168-180.

Xu, Z., Wang, Q., Dong, H., Cao, H., Li, G., Liang, F., Rai, S. M., Kylander-Clark, A., Adhikari, S. & Ji, S. (2021). Middle Eocene - Oligocene anatexis and exhumation of the Greater Himalayan Sequence in central Nepal. Terra Nova, 33, 590–601.

Yan, D., Zhou, M., Robinson, P. T., Grujic, D., Malpas, J., Kennedy, A., & Reynolds, P. H. (2012). Constraining the mid-crustal channel flow beneath the Tibetan Plateau: Data from the Nielaxiongbo gneiss dome, SE Tibet. International Geology Review, 54, 615-632.

Yang, L., Liu, X. C., Wang, J. M., & Wu, F. Y. (2019). Is Himalayan leucogranite a product by in situ partial melting of the Greater Himalayan Crystalline? A comparative study of leucosome and leucogranite from Nyalam, southern Tibet. Lithos, 342, 542-556.

Yin, A. (2006). Cenozoic tectonic evolution of the Himalayan orogen as constrained by along-strike variation of structural geometry, exhumation history, and foreland sedimentation. Earth-Science Reviews, 76, 1-131.

Yin, A. (2000). Mode of Cenozoic east-west extension in Tibet suggesting a common origin of rifts in Asia during the Indo - Asian collision. Journal of Geophysical Research: Solid Earth, 105, 21745-21759.

Yin, A., Harrison, T. M., Ryerson, F. J., Wenji, C., Kidd, W. S. F., & Copeland, P. (1994). Tertiary structural evolution of the Gangdese thrust system, southeastern Tibet. Journal of Geophysical Research: Solid Earth, 99, 18175-18201.

Zhang, J., Santosh, M., Wang, X., Guo, L., Yang, X., & Zhang, B. (2012). Tectonics of the northern Himalaya since the India–Asia collision. Gondwana Research, 21, 939-960.

https://doi.org/10.5194/egusphere-2024-2468
Preprint. Discussion started: 27 August 2024

Zhang, L., Li, G., Cao, H., Zhang, Z., Dong, S., Liang, W., Fu, J., Huang, Y., Xia, X., Dai, Z., Pei, Q. & Zhang, S. (2020). Activity of the south Tibetan detachment system: Constraints from leucogranite ages in the eastern Himalayas. Geological Journal, 55, 5540–5573.

Zhang, S., Gao, R., Li, H., Hou, H., Wu, H., Li, Q., Yang, K., Li, C., Li, W., Zhang, J., Yang, T., Keller, G. R., & Liu, M. (2014). Crustal structures revealed from a deep seismic reflection profile across the Solonker suture zone of the Central Asian Orogenic Belt, northern China: An integrated interpretation. Tectonophysics, 612, 26-39.

Zhang, Z., Wang, Y., Houseman, G. A., Xu, T., Wu, Z., Yuan, X., Chen, Y., Tian, X., Bai, Z., & Teng, J. (2014). The Moho beneath western Tibet: Shear zones and eclogitization in the lower crust. Earth and Planetary Science Letters, 408, 370-377.

Zheng, Y., Sun, X., Tian, L., Zheng, H., Yu, M., Yang, W., Zhou, T., & Geng, X. (2014). Mineralization, deposit type and metallogenic age of the gold antimony polymetallic belt in the eastern part of North Himalayan. Geotectonica et Metallogenia, 38, 108-118.

Zeng, L. S., & Gao, L. E. (2017). Cenozoic crustal anatexis and the leucogranites in the Himalayan collisional orogenic belt. Acta Petrologica Sinica, 33, 1420-1444.

Zeng, L., Gao, L., Xie, K., & Liu, Z. (2011). Mid-Eocene high Sr/Y granites in the Northern Himalayan Gneiss Domes: melting thickened lower continental crust. Earth and Planetary Science Letters, 303, 251-266.

Figures

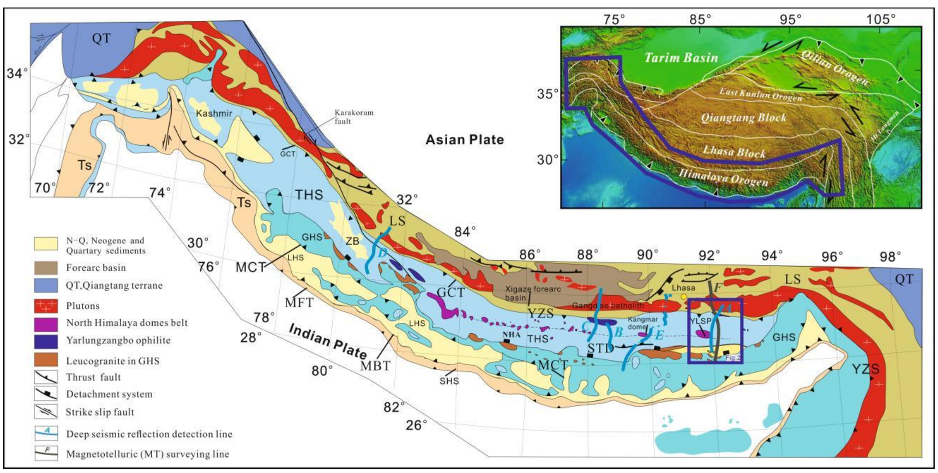

Figure 1. Geological map of the Himalayas (modified after Yin, 2006; Kapp et al., 2019; Guo et al., 2021). The blue solid line area in the upper right corner indicates the geographical location of the Himalayas within the Tibet Plateau. The digital elevation map was calculated

https://doi.org/10.5194/egusphere-2024-2468
Preprint. Discussion started: 27 August 2024

using Global Mapper software. Line A represents the seismic survey transect conducted in this study. Lines B and C represent the seismic transects by Guo et al. (2017) in the central Himalayas. Line D corresponds to the western Himalayas seismic transect by Gao et al. (2016b). Line E is the IN-DEPTH seismic line (Hauck et al., 1998), and line F is the Magnetotellurics (MT) line from the IN-DEPTH project (Spratt et al., 2005). QT-Qiangtang terrane, LS-Lhasa terrane, ZB-Zada Basin, NHA-North Himalayan antiform, YLSP-Yarlhashampo dome, GCT- Great Counter Thrust, Ts-Tertiary sediments in the foreland basin and along the Yarlung-Zangbo suture zone.

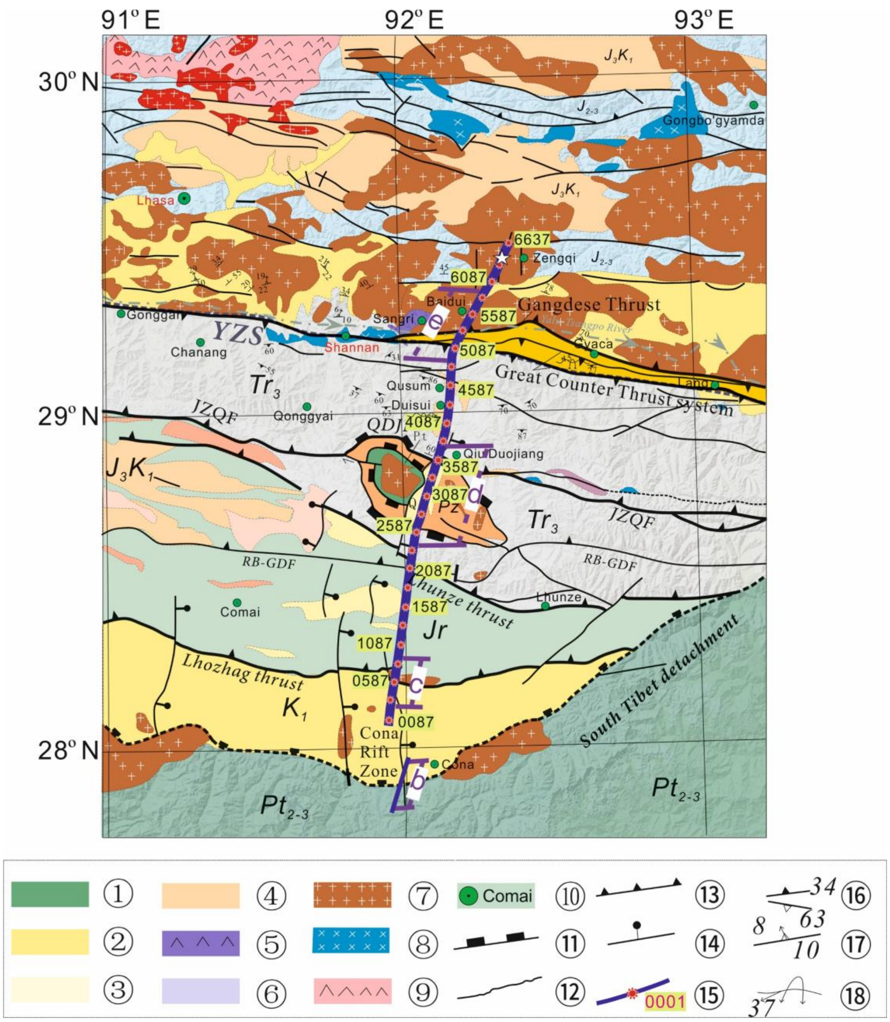

https://doi.org/10.5194/egusphere-2024-2468
Preprint. Discussion started: 27 August 2024

Figure 2. Regional geological map of the research area (modified after Dong et al., 2020). The solid blue line represents the location of deep seismic reflection profile route, with the line number indicating the corresponding CMP numbers. The routes b, c, d, and e correspond to the field geological survey routes depicted in Figure 4B, C, D, E, respectively. ①-Schist, gneiss, and eclogite strata in Meso-Neoproterozoic; ②-Sand shale, limestone, and marlite strata in early Cretaceous; ③-Quaternary deposit sediment; ④-Sand shale inclusion limestone, andesite, and shale inclusion limestone strata in late Jurassic to early Cretaceous; ⑤-Ophiolite in Cretaceous; ⑥-Sand slate contains marlite, radiolarian siliceous rock or basalt in late Triassic; ⑦-Acid intrusive rock in Cenozoic; ⑧-Intermediate and acid rock in Cretaceous; ⑨- The Lin Zizong effusive rocks; ⑩-city; ⑪- Detachment/ Normal fault; ⑫-Inferred faults; ⑬-Reversed fault; ⑭- Normal fault; ⑮- Seismic array with CMP number; ⑯- Slaty cleavage and gneissic foliation; ⑰- Mylonitic foliation in the Gangdise thrust system; ⑱- Fold and attitude of fold hinge. THS-Tethyan Himalayas, YZS-Yarlung-Zangbo suture, YLSP-Yarlhashampo dome, JZQF-Jiama-Zongxu-Qusang Fault, QDJ-Qiongduojiang Fault, RB-GDF-Rongbu-Gudui Fault.

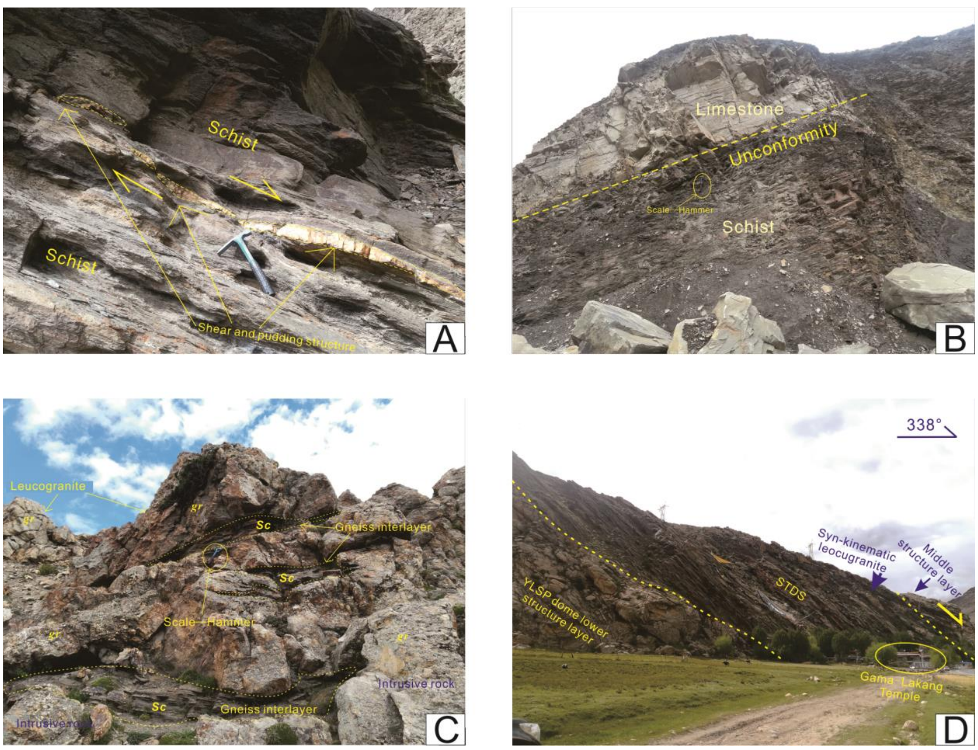

https://doi.org/10.5194/egusphere-2024-2468
Preprint. Discussion started: 27 August 2024

Figure 3. (a) North-dipping schist with quartz veins and boudin structures on the northern side of the YLSP dome. These boudins were later faulted under a shear stress field. (b) Tethys Himalaya Triassic limestone, parallel unconformably overlying the Precambrian metamorphic sequence (schist). (c) Leucogranite near the Cuona dome, incorporating some layers of gneiss and schist. (d) The STDS presents as the boundary between the lower and middle structure layers of the YLSP dome. Syn-kinematic leucogranites have developed within the schist, indicating top-to- north shearing movement. This outcrop is located on the north side of the YLSP dome, with the Gama-Lakang temple providing a reference scale. Sc-schist, gr-granite.

https://doi.org/10.5194/egusphere-2024-2468
Preprint. Discussion started: 27 August 2024

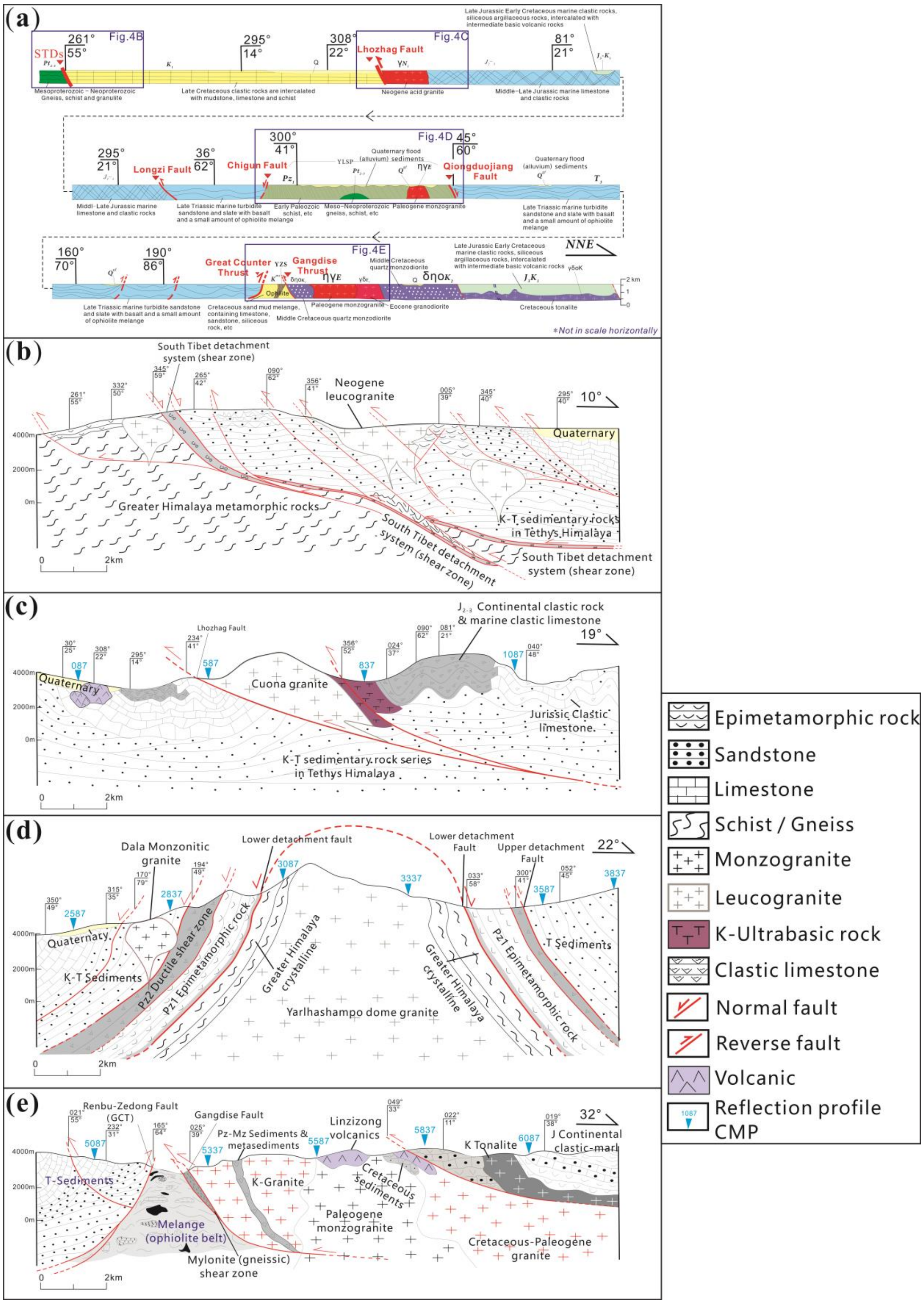

Figure 4. Geological profiles correspond to the deep seismic reflection exploration route based on field geological investigation results. (a) Overall simplified geological profile long

https://doi.org/10.5194/egusphere-2024-2468
Preprint. Discussion started: 27 August 2024

the seismic exploration route, see profile location in Figure 2; (b) Southern Tibet detachment geological section, see profile location in Figures 2 and 4A; (c) Lhozhag-Cuona geological section, see profile location in Figures 2 and 4A; (d) Yalashampoo geological section, see profile location in Figures 2 and 4A; (e) YZS-Gangdise geological section, see profile location in Figures 2 and 4A. The notation 261°/55° represents the inclination and dipping angle, respectively.

https://doi.org/10.5194/egusphere-2024-2468
Preprint. Discussion started: 27 August 2024

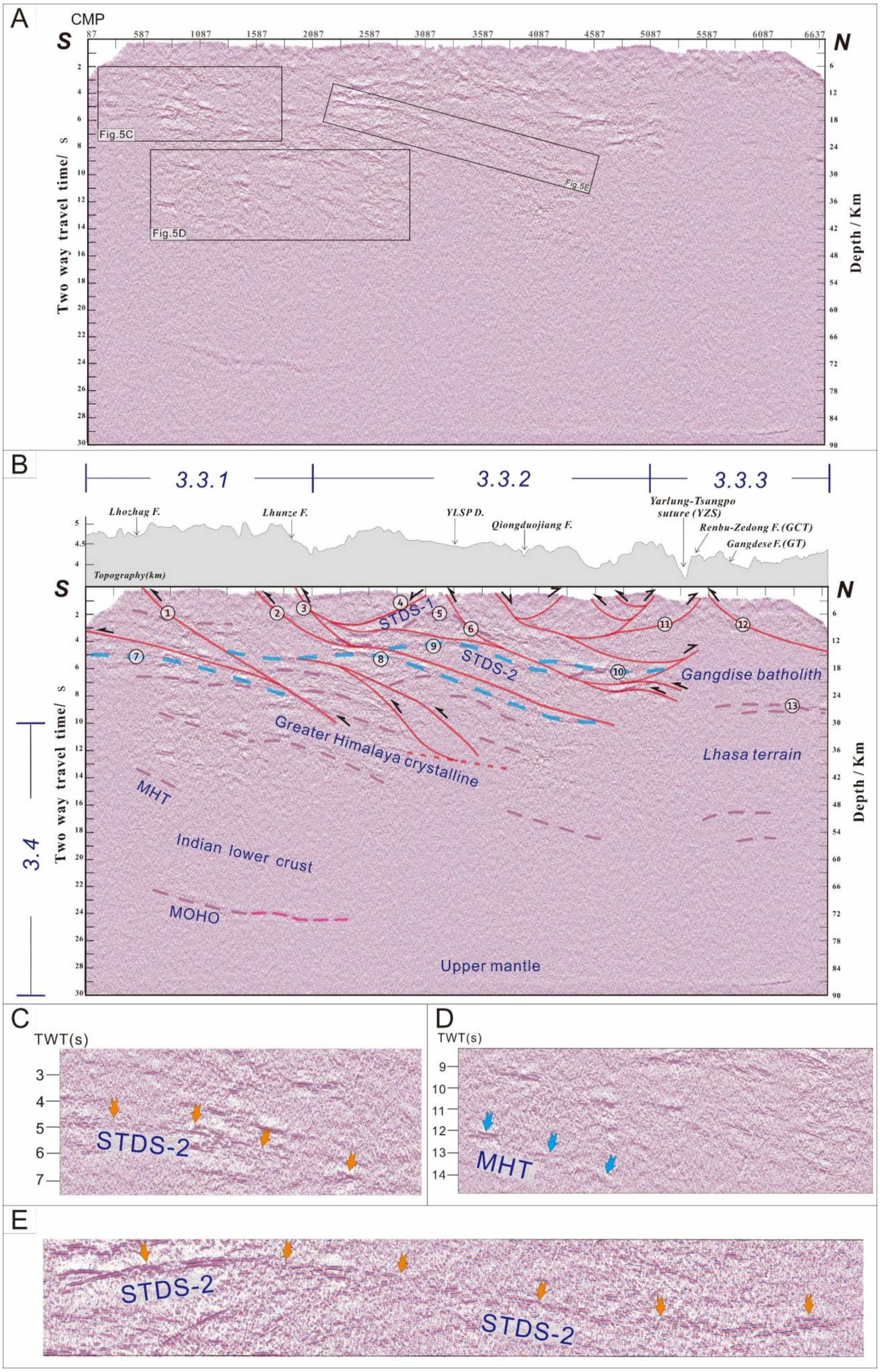

https://doi.org/10.5194/egusphere-2024-2468
Preprint. Discussion started: 27 August 2024

Figure 5. The post-stack migration seismic reflection profile. (A) Uninterpreted seismic reflection profile (no vertical exaggeration, and a crustal velocity of 6 km/s is assumed). (B) Interpreted seismic reflection profile. Notes that the solid lines for interpretation were placed on observed reflections, while dotted lines were inferred based on surface geology and reflection cutoff information. The transect surface trace is labelled as line A in Figure 1, and Figure 5 shows the surface geological map. (C) Enlarged seismic section shows the STDS-2 reflection from ca. 4-7 s TWTT in the southern part of seismic reflection profile, see location in Figure 4A. (D) Enlarged seismic section shows the MHT reflection from ca. 12-14 s TWTT in the southern part of the seismic reflection profile, see location in Figure 4A. (E) Enlarged seismic section of the STDS-2 reflection from ca. 4-10 s TWTT in the middle to northern part of seismic profile, this section has been rotated in order to fit the figure display, see location in Figure 4A. MHT-The Main Himalayan Thrust, Qiongduojiang F.-The Qiongduojiang Fault, Gangdese F.-The Gangdese Thrust, Renbu-Zedong F.-Renbu-Zedong Fault (also named as Greater Counter Thrust, GCT), Lhozhag F.-The Lhozhag Fault, Lhunze F.-The Lhunze Fault, YLSP D.-The Yarlashampo dome.

https://doi.org/10.5194/egusphere-2024-2468
Preprint. Discussion started: 27 August 2024

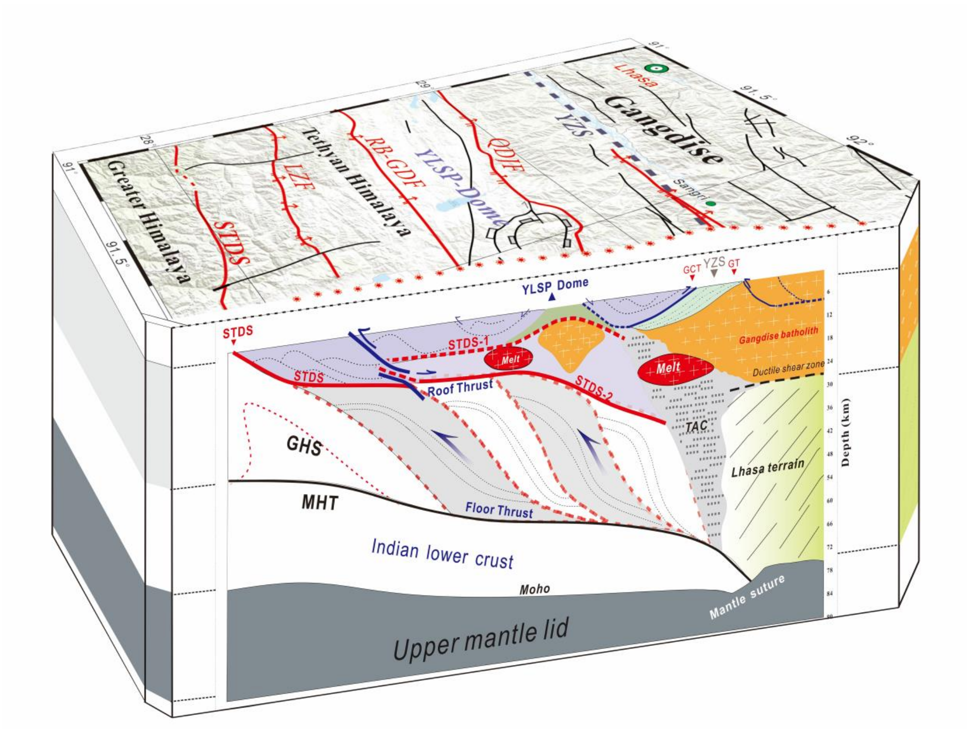

Figure 6. Structural interpretation model based on the surface geology and deep seismic reflection data. TAC-Tethyan accretionary complex, YZS-The Yarlung-Zangbo suture, YLSP-Yarlhashampo, GHS-Greater Himalayas, STDS-South Tibet Detachment System, GT-Gangdese Thrust, GCT-Greater Counter Thrust (Renbu-Zedong fault), QDJF-Qiuduojiang Fault, RB-GDF-Rongbu-Gudui Fault, LZF-Lhozhag Fault.

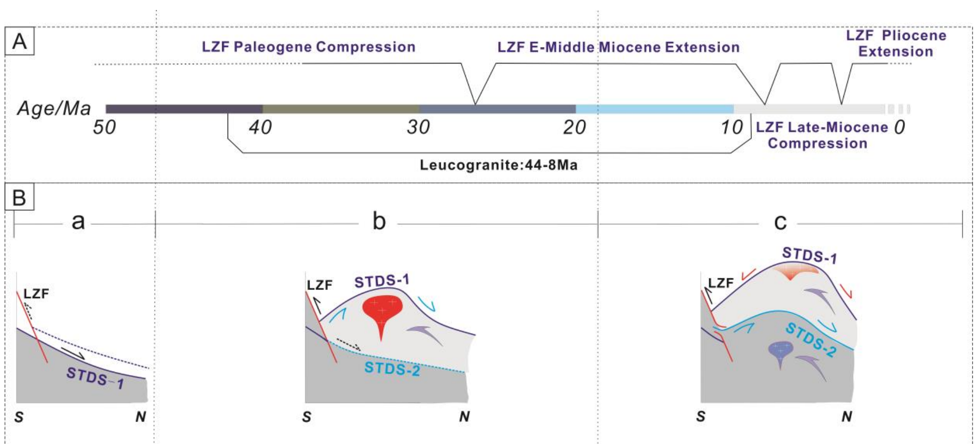

https://doi.org/10.5194/egusphere-2024-2468
Preprint. Discussion started: 27 August 2024

Figure 7. Activity timeline of the STDS, YLSP dome, and regional faults in the eastern Himalayas (not to scale). A-Timeline indicates the activation of the Lhozhag fault and the crystallization of leucogranites. B-The evolutionary sketch models correspond to timeline A, illustrating the multi-stage formation and evolution process of the STDS. The age data are summarized from Yin, 2006; Yan et al. (2012); Zhang et al. (2012); Webb, 2013; Wu et al. (2015); Kellett et al. (2018); Liu et al. (2019); Jessup et al. (2019); Zhang et al. (2020).

https://doi.org/10.5194/egusphere-2024-2468
Preprint. Discussion started: 27 August 2024

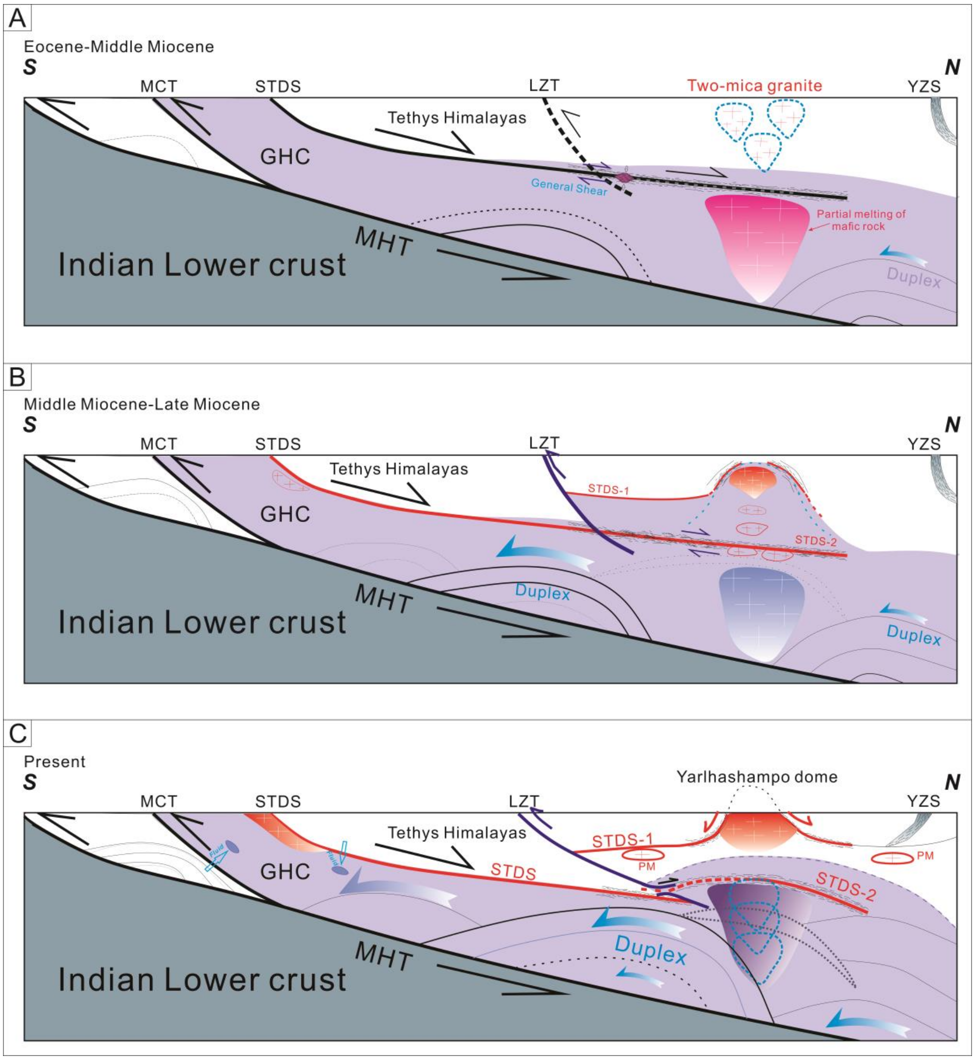

Figure 8. Tectonic evolutionary processes of the YLSP dome and associated leucogranites in the study area (not to scale). MCT-Main central thrust, YZS-Yarlungzangbo suture, LZT-Lhozhag fault, MHT-Main Himalayan Thrust, GHC- Greater Himalayan complex, PM-Partial melts, STDS-Southern Tibet Detachment System. See context for description in detail.